Supporting Information:

Revealing the underlying absorption and emission mechanism of nitrogen ~~doping~~ graphene quantum dots

Xianghong Niu[1], Yunhai Li[1], Huabing Shu[1] and Jinlan Wang*[1,2]

[1]*Department of Physics, Southeast University, Nanjing 211189, China*

[2]*Synergetic Innovation Center for Quantum Effects and Applications (SICQEA), Hunan Normal University, Changsha 410081, China*

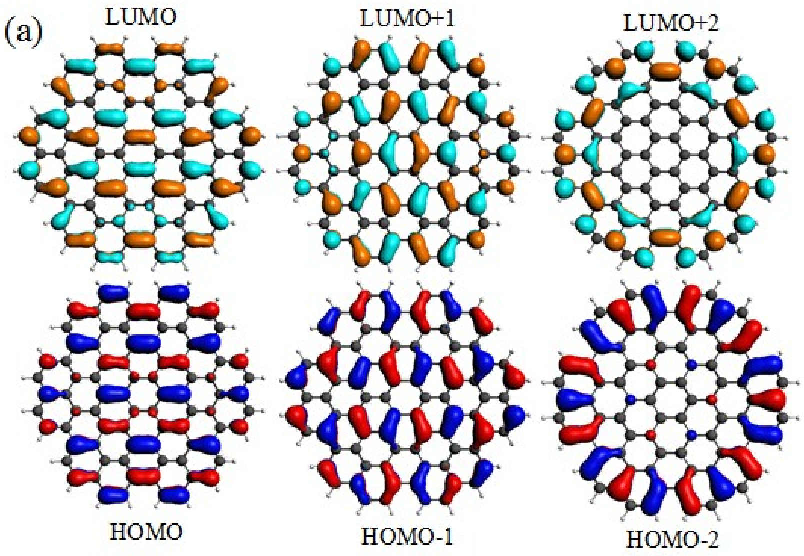

Figure S1. Frontier orbitals of the pristine GQD that dominate mainly optical transitions.

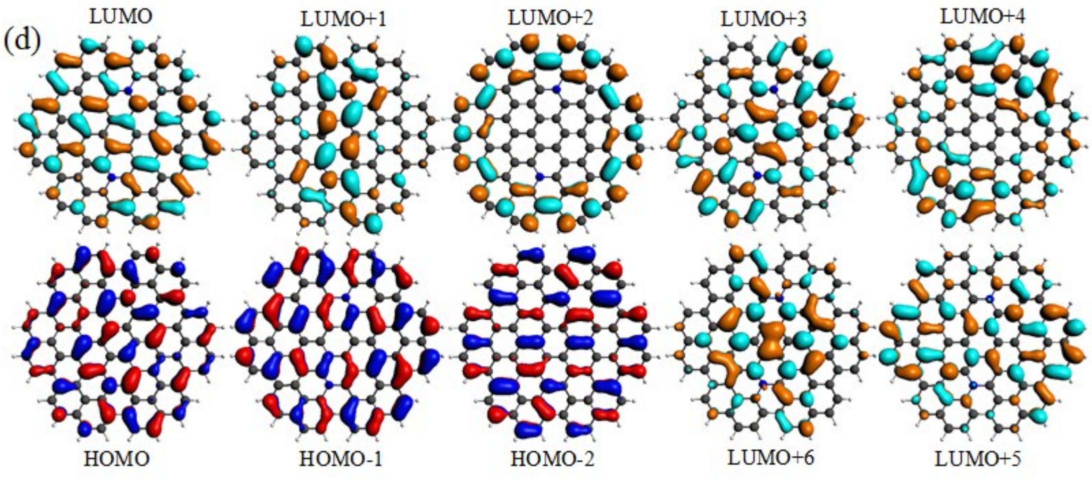

Figure S2. Frontier orbitals of the graphitic N-~~doping~~ GQD that dominate mainly optical transitions.

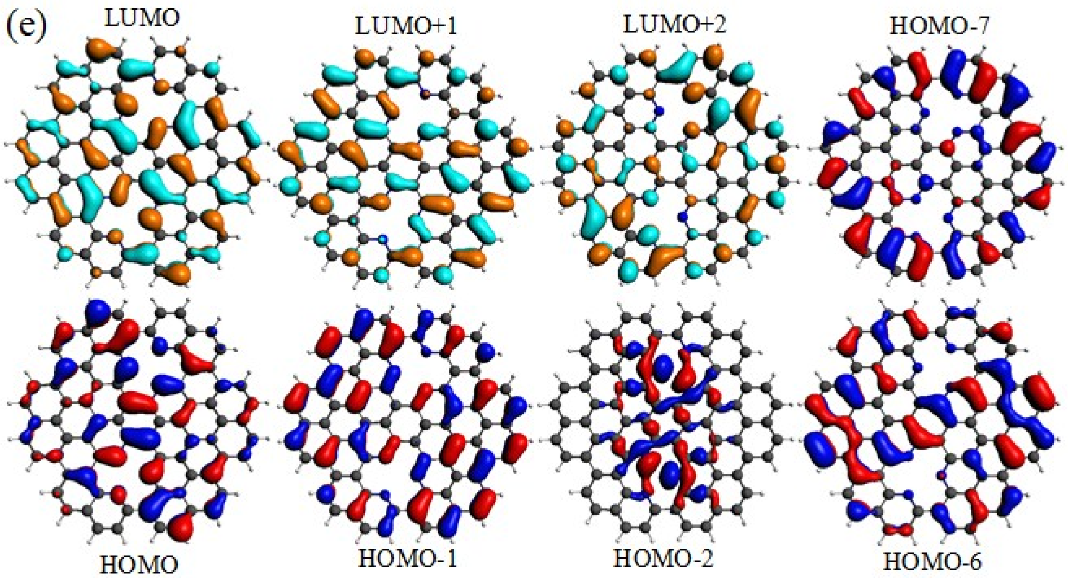

Figure S3. Frontier orbitals of the pyridinic ~~at center N-doping~~ GQD that dominate mainly optical transitions.

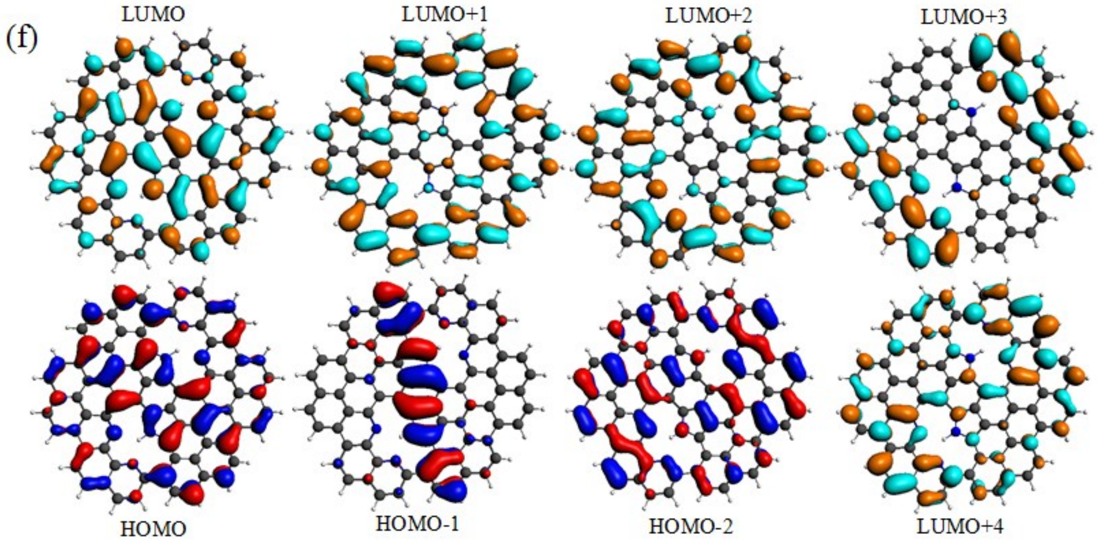

Figure S4. Frontier orbitals of the pyrrolic ~~at center N-doping~~ GQD that dominate mainly optical transitions.

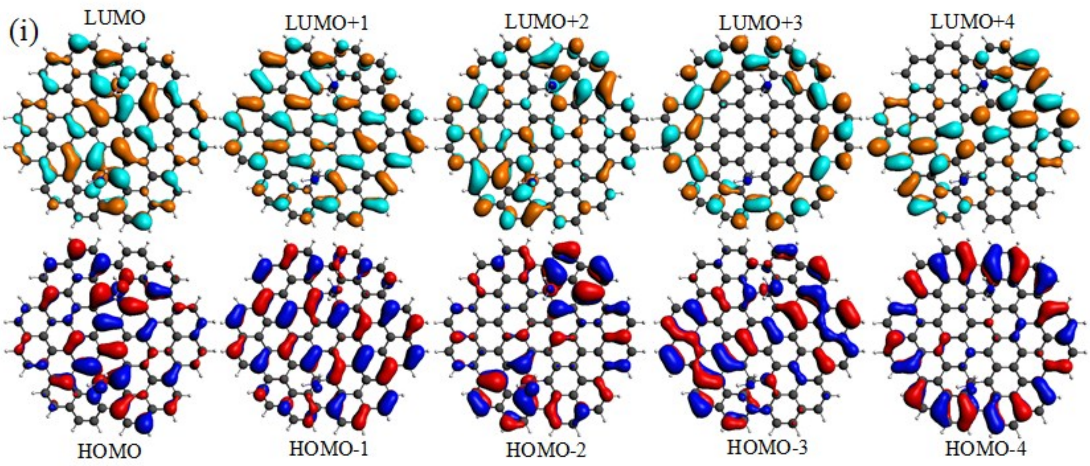

Figure S5. Frontier orbitals of the ~~amido at center N-doping~~ GQD that dominate mainly optical transitions.

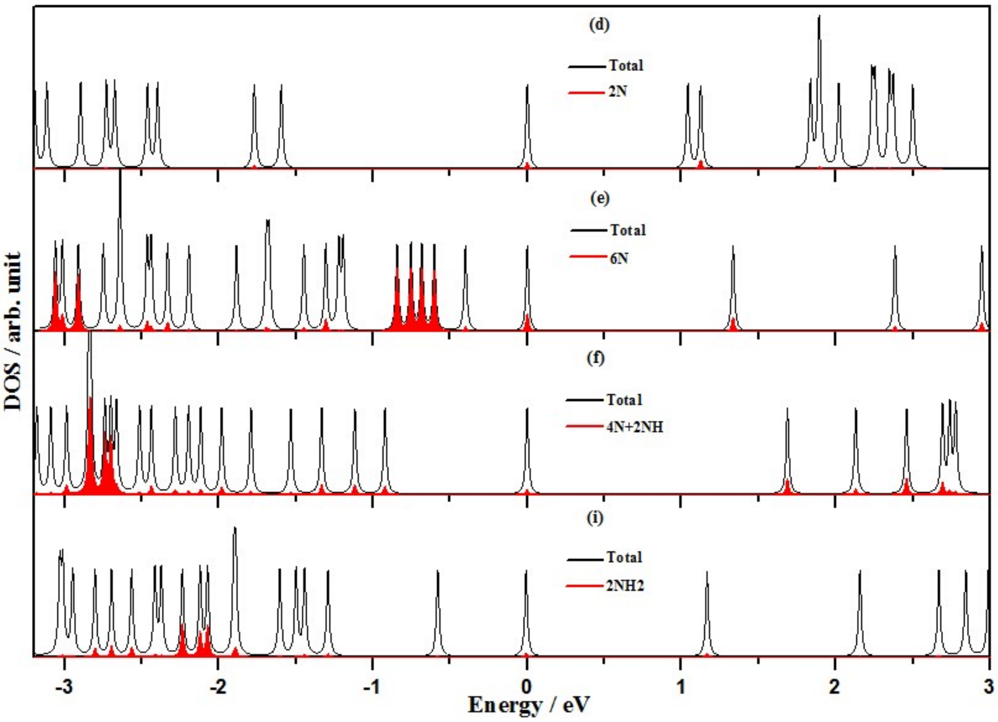

Figure S6. The density of states (DOSs) of four type N-GQDs (d, e, f, i). The Fermi energy is set at zero. Black line represents total DOSs, and the region of red represents N-doping PDOSs, respectively. The DOSs are plotted with a Lorentzian width of 0.01 eV.

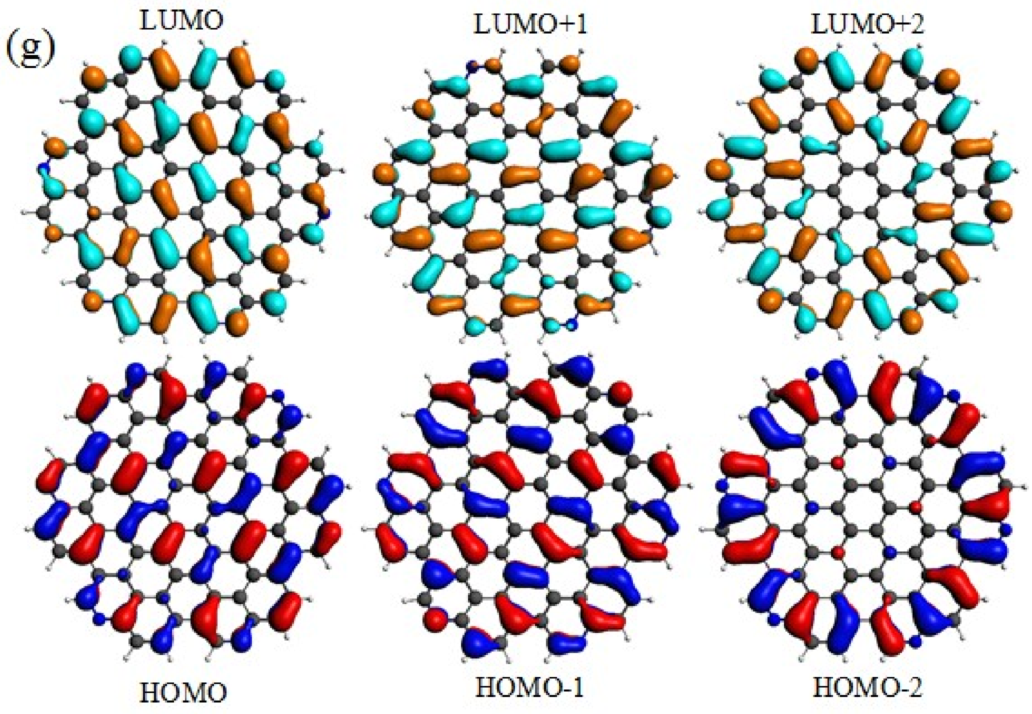

Figure S7. Frontier orbitals of the pyridinic ~~at edge N-doping~~ GQD (g) that dominate mainly optical transitions.

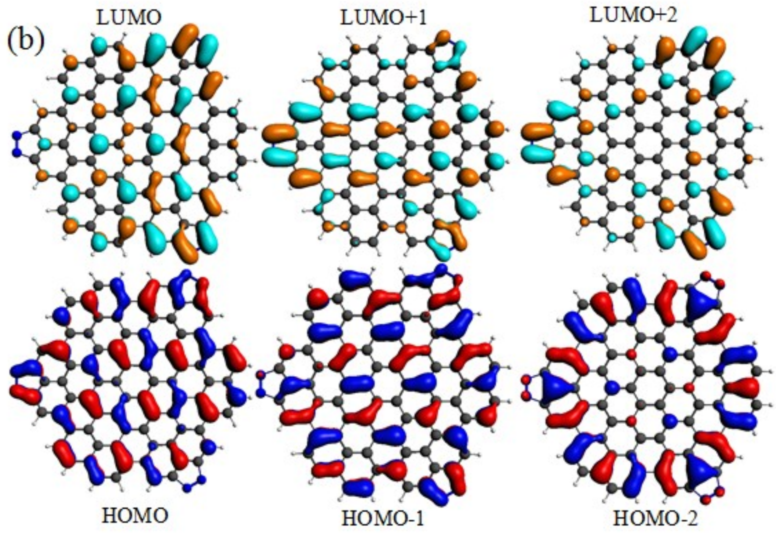

Figure S8. Frontier orbitals of the pyrazole N-~~doping~~ GQD that dominate mainly optical transitions.

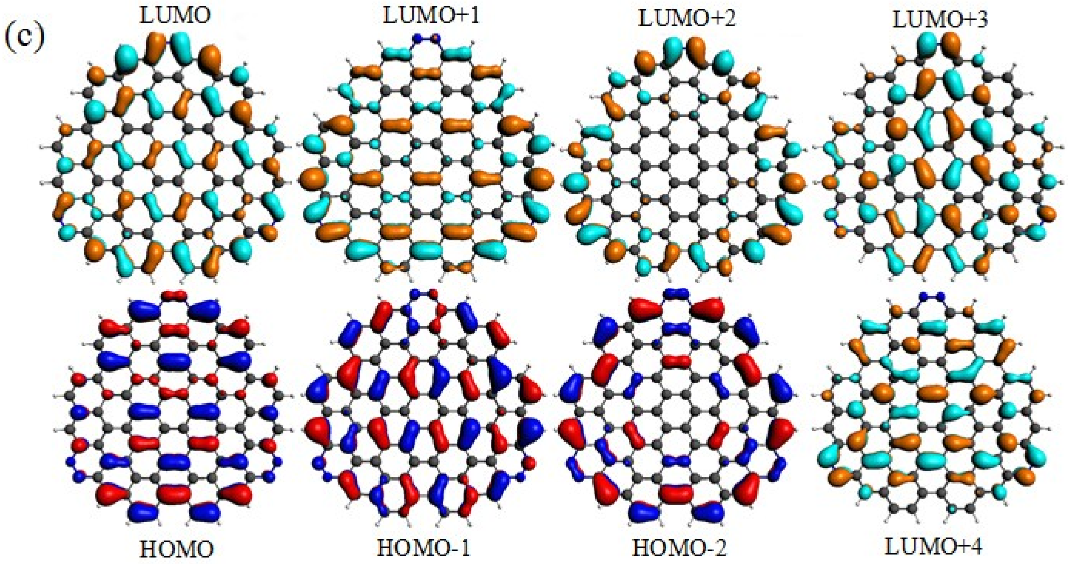

Figure S9. Frontier orbitals of the pyridazine N-~~doping~~ GQD that dominate mainly optical transitions.

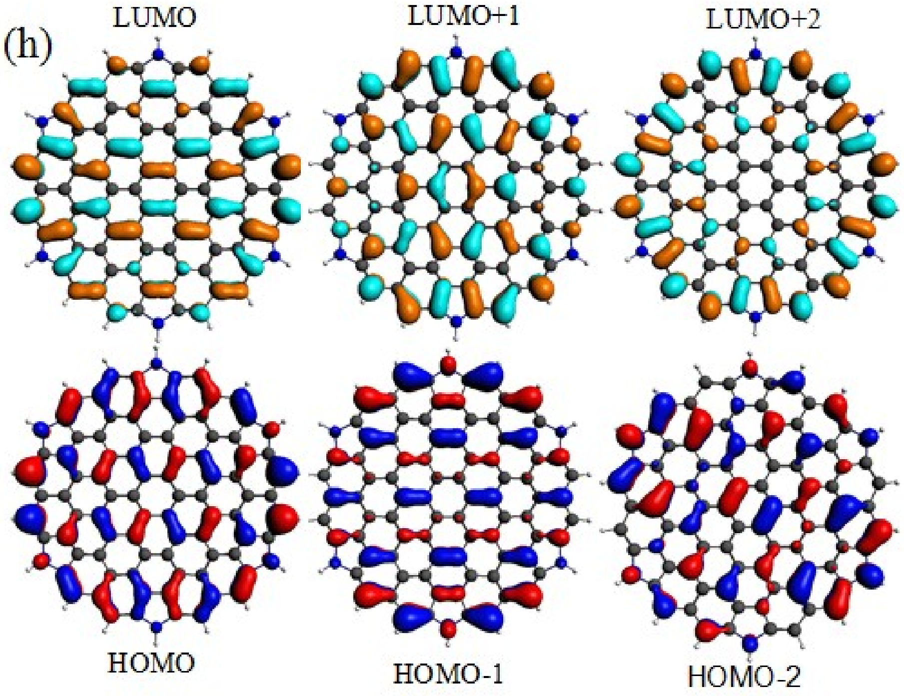

Figure S10. Frontier orbitals of the pyrrolic ~~at edge N-doping~~ GQD that dominate mainly optical transitions.

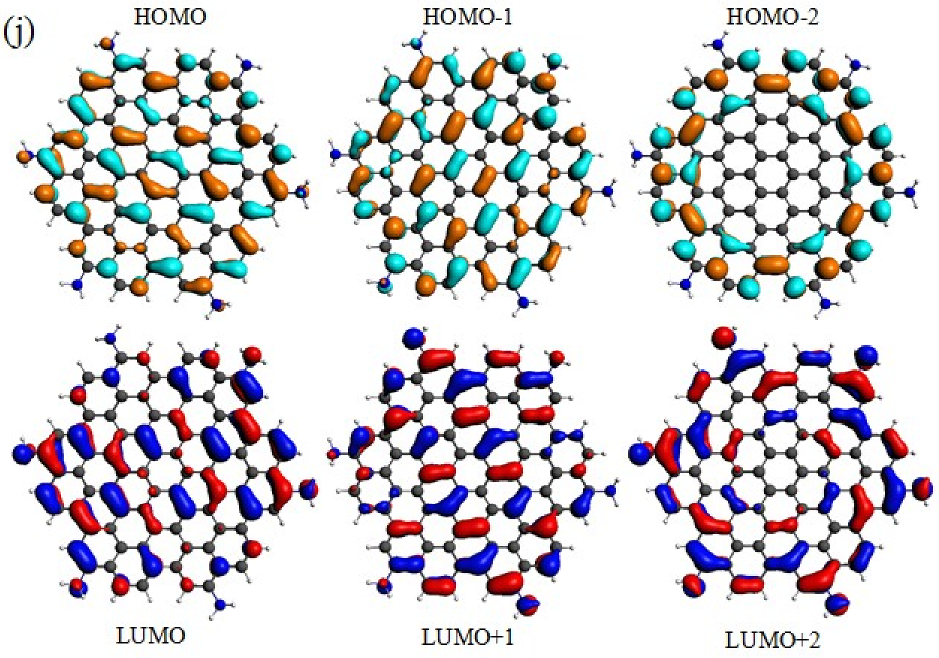

Figure S11. Frontier orbitals of the ~~amido at edge N-doping~~ GQD that dominate mainly optical transitions.

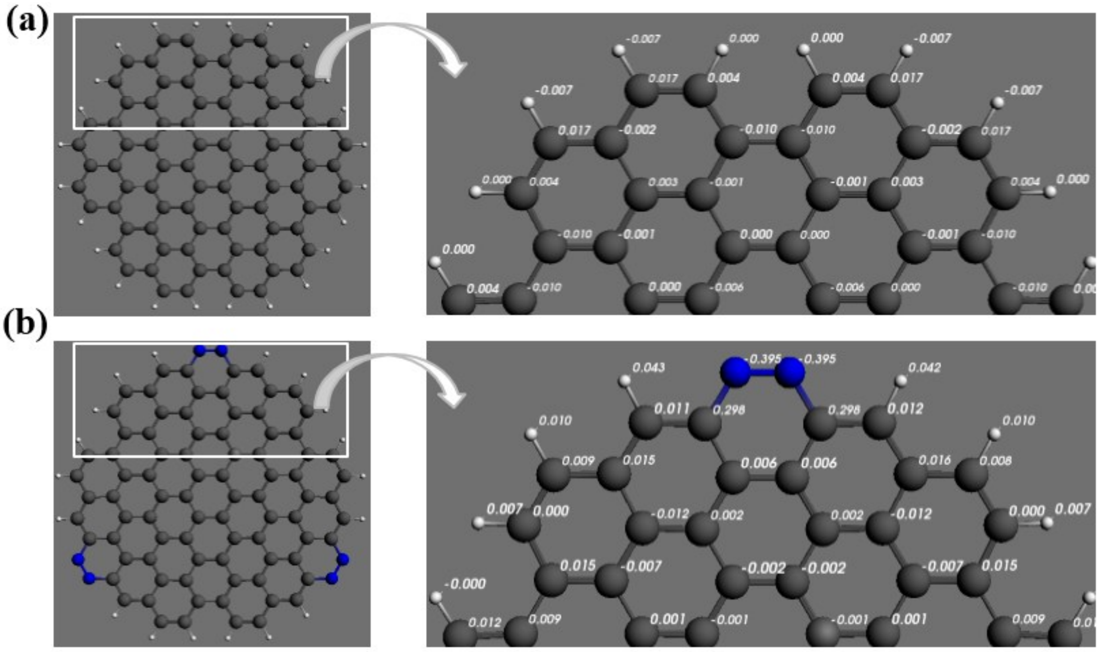

Figure S12. Charge densities of each atom in (a) pristine GQD and (b) the pyridazine N-doping GQD (only the part atoms around doping nitrogen atoms are presented). Atomic color code: black, carbon; white, hydrogen; and blue, nitrogen.

The analysis of orbital hybridization

According to the basic knowledge on chemical bonding theory, supposing that to the system contain two atoms labelled as *A* and *B*, and each carries one orbital (φ_A and φ_B) and the corresponding orbital energies are ε_A and ε_B, then the molecular orbital can be expanded as the linear combination of φ_A and φ_B

$$\varphi = c[\varphi_A + \lambda\varphi_B], \tag{1}$$

where *c* is the normalization coefficient and λ is expansion coefficient on φ_B. Substituting φ into the Schrödinger's equation, we have

$$[-\frac{\hbar^2}{2m}\nabla^2 + V_A + V_B]\, c[\varphi_A + \lambda\varphi_B] = \varepsilon \cdot c[\varphi_A + \lambda\varphi_B]. \tag{2}$$

Introducing that

$$\begin{cases} H_{aa} = \int \varphi_A^* H \varphi_A dr \approx \varepsilon_A \\ H_{bb} = \int \varphi_B^* H \varphi_B dr \approx \varepsilon_B \\ H_{ab} = \int \varphi_A^* H \varphi_B dr = \int \varphi_B^* H \varphi_A dr = H_{ba} \end{cases} \tag{3}$$

we can rewrite equation (2) in the matrix form

$$\begin{bmatrix} H_{aa} & H_{ab} \\ H_{ab} & H_{bb} \end{bmatrix} \begin{bmatrix} 1 \\ \lambda \end{bmatrix} = \varepsilon \begin{bmatrix} 1 \\ \lambda \end{bmatrix}. \tag{4}$$

Diagonalization of the Hamiltonian yields

$$\begin{cases} \varepsilon^+ = \dfrac{\varepsilon_A + \varepsilon_B}{2} - \sqrt{V_2^2 + V_3^2} \\ \varepsilon^- = \dfrac{\varepsilon_A + \varepsilon_B}{2} + \sqrt{V_2^2 + V_3^2} \\ \lambda^+ = \dfrac{\sqrt{V_2^2 + V_3^2} - V_3}{V_2} \\ \lambda^- = \dfrac{\sqrt{V_2^2 + V_3^2} + V_3}{V_2} \\ V_2 = -H_{ab} \\ V_3 = \dfrac{\varepsilon_B - \varepsilon_A}{2} \end{cases}, \tag{5}$$

where $\varepsilon^+(\varepsilon^-)$ and $\lambda^+(\lambda^-)$ are the energy and for bonding (anti-bonding) states, respectively.

As λ describes the expansion coefficient, its squared modulus λ^2 is thus the contribution of φ_B on molecular orbital φ. If $\lambda \to 0$ or $\lambda \to \infty$, then φ is totally composed by either φ_A or φ_B, indicating no hybridization, while $\lambda \to 1$ indicates the maximal hybridization. This inspires us to use λ as the hybridization indicator and define

$$\frac{(\lambda^+)^2}{(\lambda^-)^2} = \left(\frac{\lambda^+}{\lambda^-}\right)^2 = \left(\frac{\sqrt{V_2^2 + V_3^2} - V_3}{\sqrt{V_2^2 + V_3^2} + V_3}\right)^2 . \tag{6}$$

In the **even hybridization** case, φ_B has equal contribution on both bonding and anti-bonding states. Thus $(\lambda^+)^2$ should approximately be equal to $(\lambda^-)^2$, and we have $(\lambda^+)^2 / (\lambda^-)^2 \approx 1$. In the **uneven hybridization** case, φ_B mainly constitutes either the bonding or anti-bonding states, and we have $(\lambda^+)^2 / (\lambda^-)^2 > 1$ or $(\lambda^+)^2 / (\lambda^-)^2 < 1$, respectively.

From equation (5) the energy gap can be easily obtained

$$E_g = 2\sqrt{V_2^2 + V_3^2} . \tag{7}$$

Note that $E_g > 2|V_3|$. Substituting equation (7) into (6), we finally have the relation between energy gap and orbital hybridization

$$\frac{(\lambda^+)^2}{(\lambda^-)^2} = \left(1 - \frac{4V_3}{E_g + 2V_3}\right)^2 . \tag{8}$$

For $V_3 > 0$, we have $(\lambda^+)^2 / (\lambda^-)^2 < 1$. As demonstrated in Figure R1, E_g increases as $(\lambda^+)^2 / (\lambda^-)^2$ approaches 1, showing asymptotic behavior. For $V_3 < 0$, we have $(\lambda^+)^2 / (\lambda^-)^2 > 1$, and E_g also increases as $(\lambda^+)^2 / (\lambda^-)^2 \to 1$.

Now it's clear that **even hybridization** ($(\lambda^+)^2 / (\lambda^-)^2 \approx 1$) indicates a large energy gap, while **uneven hybridization** ($(\lambda^+)^2 / (\lambda^-)^2$ far away from 1) indicates a smaller gap.

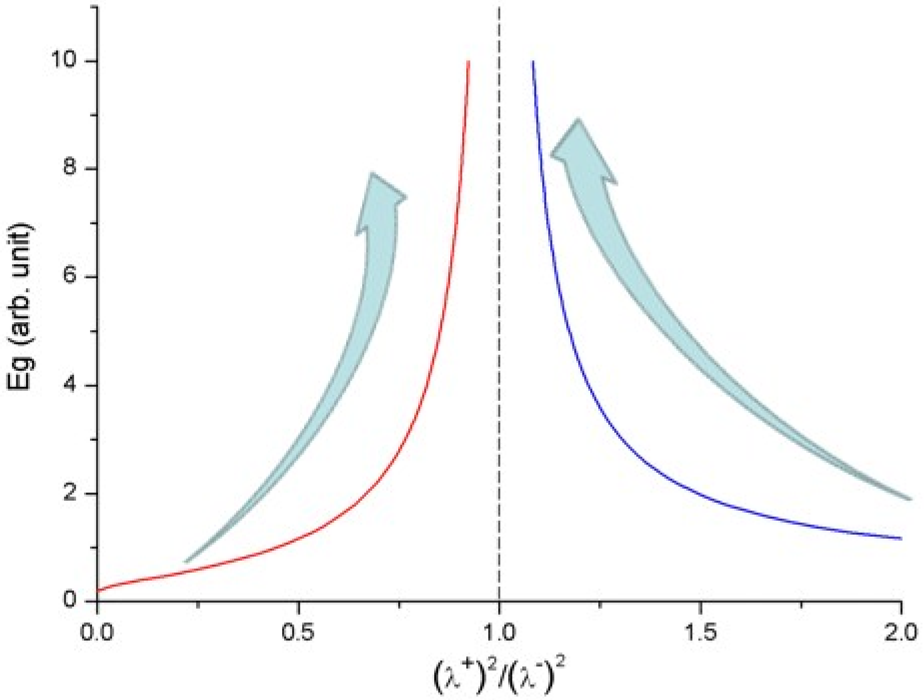

Figure S13. Schematic plot of E_g against $(\lambda^+)^2/(\lambda^-)^2$. Red and blue solid lines indicate the figure for V_3 = 0.1 and -0.1, respectively. The black dash line indicates the asymptotic line. Both E_g and V3 are in arbitrary units.

As shown in Figure 5, nitrogen-containing group mainly constitutes HOMO rather than LUMO for pyrazole (b) and pyridazine (c) structures, while for pyrrolic (h) and amino (j) it is the opposite. As aforementioned, this indicates the change in the sign of V_3 from positive for (b) and (c) to negative for (h) and (j), which changes the behavior of the function of E_g against $(\lambda^+)^2/(\lambda^-)^2$.

From equation (8) we have $\lim_{x\to 0^+} E_g = 0$ and $\lim_{x\to +\infty} E_g = 0$, where x is the shorthand for $(\lambda^+)^2/(\lambda^-)^2$. As E_g converges to 0 within $[0,1]$ for $V_3 > 0$ while the converging range is $[0,+\infty)$ for $V_3 > 0$, the function decays much faster if V_3 is positive, as demonstrated in Figure S13. This means if the nitrogen-containing group mainly constitutes HOMO rather than LUMO, the energy gap will be more sensitive to orbital hybridization than the opposite situation. Although the hybridization for (h) and (j) is more uneven than (b) and (c), their relationship of E_g on orbital hybridization is less sensitive than (b) and (c), leading to a larger energy gap.

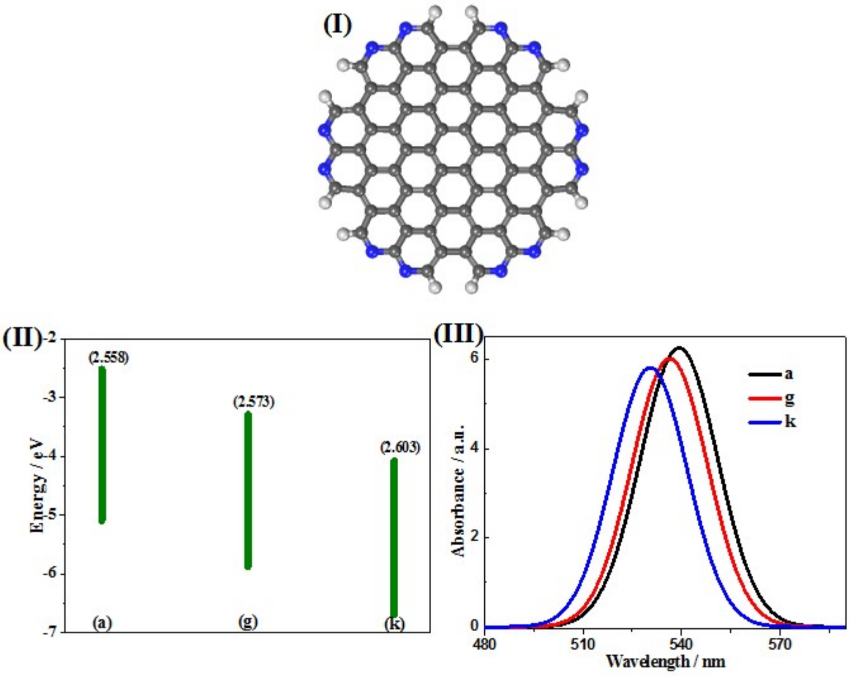

Figure S14. (I) Structure of pyridinic at edge N-GQD (k). Atomic color code: gray, carbon; blue, oxygen; white, hydrogen. (II) the HOMO-LUMO gap of pristine GQD (a) and pyridinic at edge N- GQDs (g and k). (III) Absorption spectrum of the pristine GQD (a) and pyridinic at edge N-GQDs (g and k) in THF. Each transition is convoluted with a Lorentzian broadening of 0.25 eV to generate the simulated spectrum.

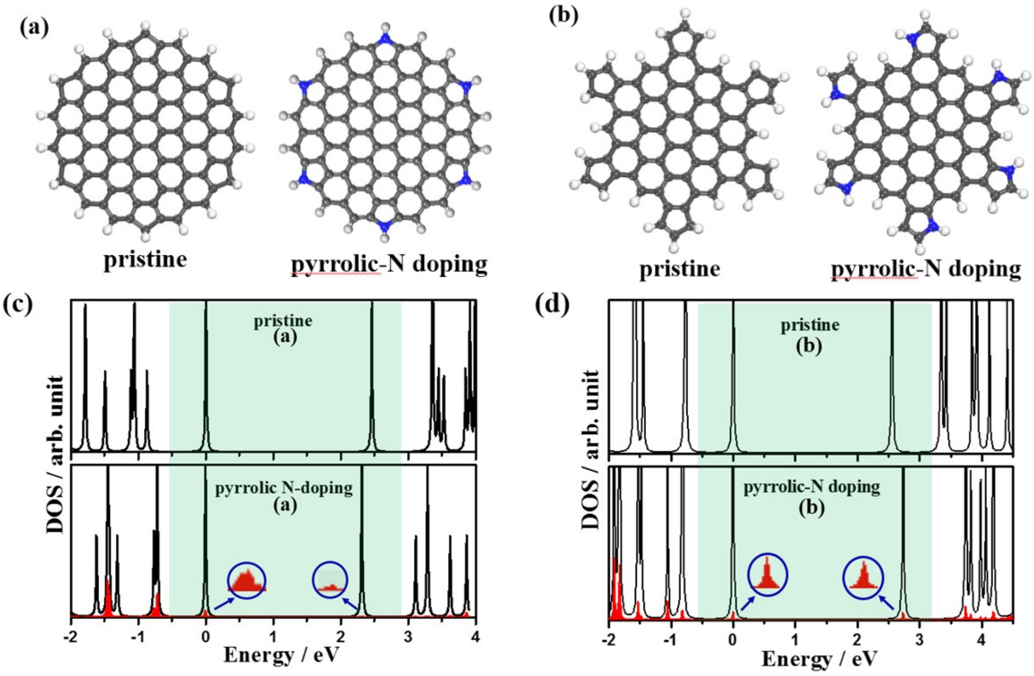

Figure S15. (a) Our pyrrolic N-doping structure; (b) Chen's pyrrolic N-doping structure from JMCC 2014, 2, 6954. (c) & (d): The DOS of pristine GQD and N-GQDs for (a) & (b), respectively. Black and red lines represent total DOS and PDOS from N, respectively. The embedded figure is the magnifying PDOS of N-~~doping~~ atoms, and the magnifying multiples are the same for all N-doping types. The low energy transitions are mainly dominated by the energy region of green. The DOS is plotted with a Lorentzian width of 0.01 eV.

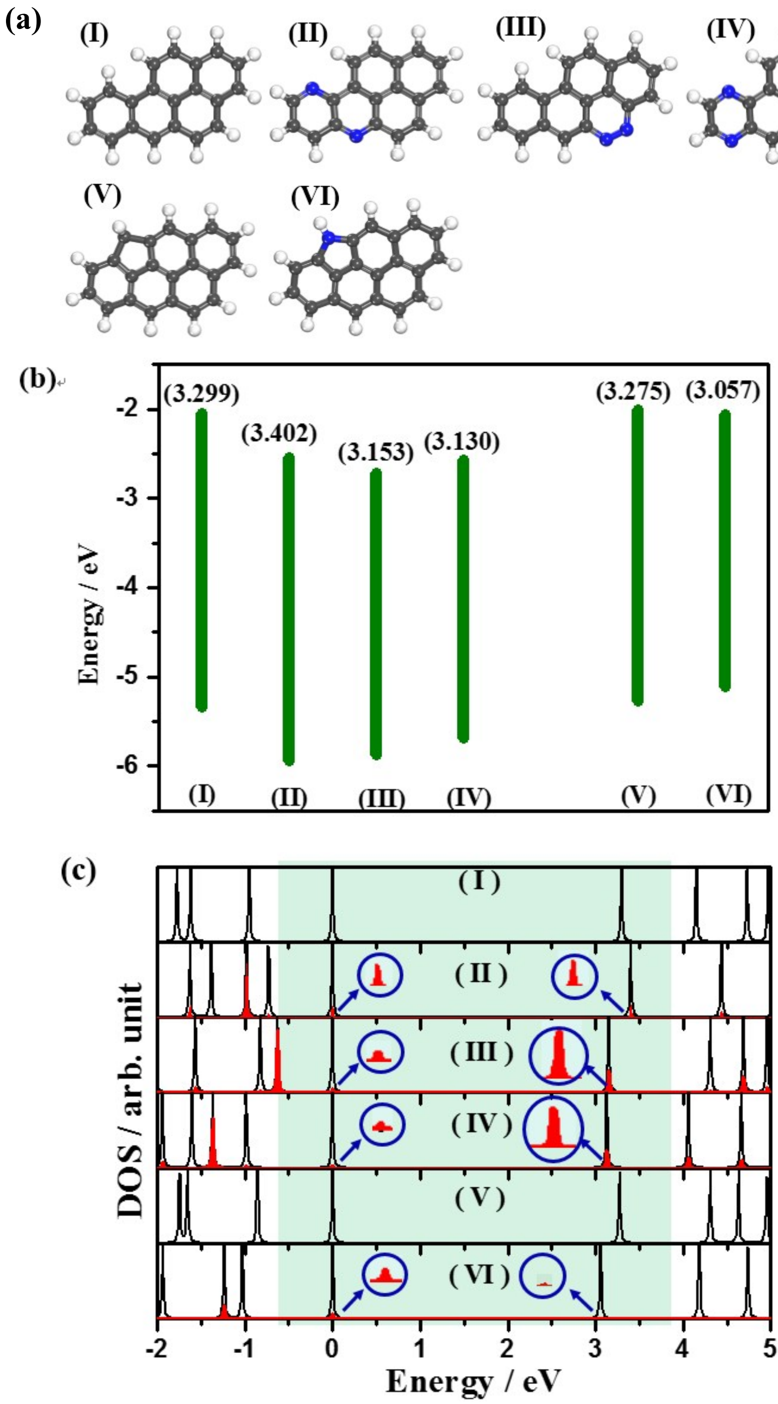

Figure S16. (a) Optimized structures of pristine GQD (I), pyridinic at edge N-GQD (II), pyridazine N-GQD (III), counterpoint N-GQD (IV), pristine of pyrrolic GQD (V) and pyrrolic at edge N-GQD (VI); (b) The HOMO-LUMO gap. (c) The DOS of pristine GQD and edge N-GQDs, respectively. The Fermi level is set to be zero. Black and red lines represent total DOS and PDOS from N, respectively. The embedded figure is the magnifying PDOS of N-~~doping~~ atoms, and the magnifying multiples are the same for all N-~~doping~~ types. The low energy transitions are mainly dominated by the energy region of green. The DOS is plotted with a Lorentzian width of 0.01 eV.

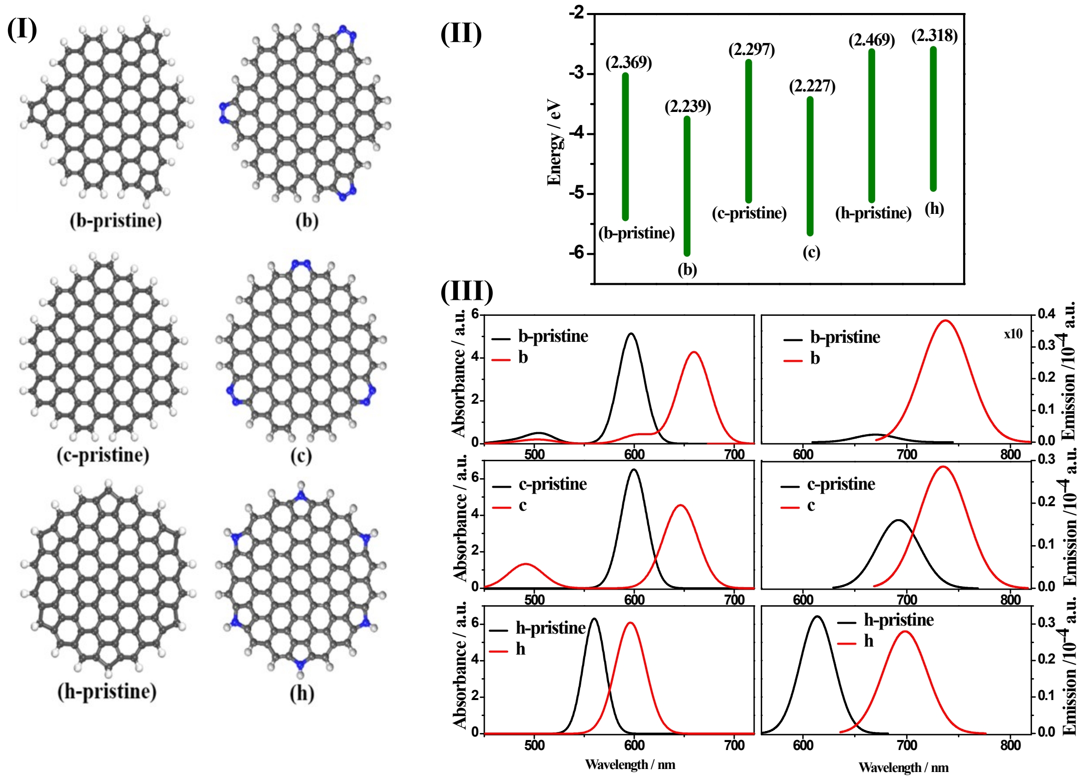

Figure S17. (I) The structures of pristine GQDs for (b) pyrazole, (c) pyridazine and (h) pyrrolic N-dop~~ing~~ type, respectively, for more refined comparison. (II) The HOMO-LUMO gap. (III) Absorption and emission spectra.

To understand the effect of N-doping in GQDs，we have used a single pristine GQD (Fig. 1) as the reference for all types of doping. Whereas, the reference may cause misunderstanding for (b) pyrazole, (c) pyridazine and (h) pyrrolic edge N-~~doping~~ type due to the different edge configurations. To give a clear picture on this issue, we also reconstructed other pristine GQDs for (b) pyrazole, (c) pyridazine and (h) pyrrolic edge N-~~doping~~ types. We find that these N-doping still decrease the HOMO-LUMO gap and lead to the red-shifted of absorption and emission spectra.